

Transient dynamics of subradiance and superradiance in open optical ensembles

Elliot Lu,^{1,2} B. Shanker,² and Carlo Piermarocchi¹

¹*Department of Physics and Astronomy, Michigan State University, East Lansing, Michigan 48824*

²*Department of Electrical & Computer Engineering,
Michigan State University, East Lansing, Michigan, 48824*

(Dated: May 16, 2022)

We introduce a computational Maxwell-Bloch framework for investigating out of equilibrium optical emitters in open cavity-less systems. To do so, we compute the pulse-induced dynamics of each emitter from fundamental light-matter interactions and self-consistently calculate their radiative coupling, including phase inhomogeneity from propagation effects. This semiclassical framework is applied to open systems of quantum dots with different density and dipolar coupling. We observe that signatures of superradiant behavior, such as directionality and faster decay, are weak for systems with extensions comparable to $\lambda/2$. In contrast, subradiant features are robust and can produce long-term population trapping effects. This computational tool enables quantitative investigations of large optical ensembles in the time domain and could be used to design new systems with enhanced superradiant and subradiant properties.

Superradiance and subradiance in optical systems continue to be under intense experimental and theoretical investigations, both in atomic and solid-state systems [1, 2]. Theoretical descriptions of these phenomena often rely on effective Hamiltonians, such as the Dicke model, where interaction with one or few cavity modes is assumed and emitters are homogeneous. For extended systems, Maxwell-Bloch equations can be used where the electric field couples to a continuous local-averaged polarization field [3, 4]. However, to understand these collective phenomena, it is essential to consider the role of the emitters' local configuration and their spatial and energy distribution. In fact, the disorder in the local distribution of the emitters can strongly affect the superradiant and subradiant dynamics. The coupling between emitters resulting from the exchange of virtual photons, known as van-der-Waals coupling [5], has been recognized for a long time to be an obstacle to the experimental observation of superradiant behavior [6]. Far from being a limitation, subradiance has been recently proposed as a mechanism for photon storage in quantum memories and the generation of entanglement-rich collective states [7, 8]. To design new systems that exploit superradiance and subradiance, we need analysis methods that: (1) simulate individual optical emitters and their mutual coupling, (2) include the full spatial dependence of the electromagnetic coupling in three dimensions, and (3) describe the dynamics in the time domain taking into account pulse-induced transients and finite propagation times.

Here, we propose a computational approach to investigate superradiant and subradiant dynamics taking into account local inhomogeneities, propagation effects, and the full spatial dependence of the electromagnetic coupling [9]. The method relies on an integral formulation of semiclassical microscopic Maxwell-Bloch equations [10].

The numerical solution of such a large number of coupled and time-delayed nonlinear equations in a random medium is challenging [11, 12], and our methods presented in detail in [13] amortize computational cost and convergence. In this approach, the nonlinear dynamics of each emitter and the field generated by the emitters' polarization are self-consistently computed, showing a rich phenomenology of short- and long-lived excitations and synchronized oscillations. Since the local configuration of emitters can be engineered in solid-state systems, we consider parameters typical of semiconductor quantum dot systems embedded in a solid matrix, which exhibit strong dipoles and where collective radiative effects have been experimentally observed [14–17]. However, the computational framework is sufficiently general so as enable exploration of other systems such as optical centers in solids and atomic clouds.

Model. We model each emitter as a two level system interacting with a classical electric field. A collection of density matrices ρ^i represents the quantum state of each dot i , and their evolution is governed by the Liouville equations $\hbar\dot{\rho}^i = -i[\mathcal{H}^i(t), \rho^i] - \mathcal{D}[\rho^i]$, where \mathcal{H}^i is the Hamiltonian of the i -th dot of energy $\hbar\omega_0^i$ and Rabi coupling $\chi^i(t) = \mathbf{d} \cdot \mathbf{E}(\mathbf{r}_i, t)$, with \mathbf{d} being the dot's transition dipole, and $\mathbf{E}(\mathbf{r}_i, t)$ the total electric field at the position of the dot, \mathbf{r}_i . The Lindblad term $\mathcal{D}[\rho^i]$ describes population decay and decoherence, parametrized by T_1 and T_2 . The key idea is solving for the total electric field, $\mathbf{E}(\mathbf{r}, t) = \mathbf{E}_L(\mathbf{r}, t) + \mathfrak{F}\{\mathbf{P}(\mathbf{r}, t)\}$, self consistently with the Liouville equation. Here $\mathbf{E}_L(\mathbf{r}, t)$ is the exciting laser field oscillating at frequency ω_L . The second term, $\mathfrak{F}\{\mathbf{P}(\mathbf{r}, t)\}$, is the radiation electric field due to a polarization distribution $\mathbf{P}(\mathbf{r}, t)$ arising from the off-diagonal elements (coherences) of the ρ^i from all the dots. The latter can be written explicitly in integral operator form:

$$\begin{aligned} \tilde{\mathfrak{F}}\{\mathbf{P}(\mathbf{r}, t)\} &\doteq -\mu_0(\partial_t^2 \mathbf{I} - c^2 \nabla \nabla)g(\mathbf{r}, t) \star_{st} \mathbf{P}(\mathbf{r}, t) \\ &= \frac{-1}{4\pi\epsilon} \int \left[(\mathbf{I} - \bar{\mathbf{r}} \otimes \bar{\mathbf{r}}) \cdot \frac{\partial_t^2 \mathbf{P}(\mathbf{r}', t_R)}{c^2 R} + (\mathbf{I} - 3\bar{\mathbf{r}} \otimes \bar{\mathbf{r}}) \cdot \left(\frac{\partial_t \mathbf{P}(\mathbf{r}', t_R)}{cR^2} + \frac{\mathbf{P}(\mathbf{r}', t_R)}{R^3} \right) \right] d^3 \mathbf{r}' \end{aligned} \quad (1)$$

where $\mathbf{R} = \mathbf{r} - \mathbf{r}'$, $t_R = t - R/c$, $\bar{\mathbf{r}} = \mathbf{R}/R$, $g(\mathbf{r}, t) = \delta(t_R)/R$ is the wave equation Green's function, \star_{st} denotes convolution in space and time, and $\mathbf{P}(\mathbf{r}, t) = \sum_i \delta(\mathbf{r} - \mathbf{r}_i) \mathbf{d} \mathfrak{R} \mathfrak{c}(2\rho_{01}^i(t))$. Solving these equations consistently is effected via an exponential predictor-corrector scheme [18].

To effect computational speedup, we transform the equations to a frame co-rotating with the laser frequency ω_L by writing $\tilde{\rho} = U \rho U^\dagger$, where $U = \text{diag}(1, e^{i\omega_L t})$. The equivalent of Eq. (1) in this rotating frame is

$$\tilde{\mathfrak{F}}\{\tilde{\mathbf{P}}\} \doteq -\mu_0(\partial_t^2 \mathbf{I} - c^2 \nabla \nabla)g(\mathbf{r}, t) \star_{st} \tilde{\mathbf{P}} e^{i\omega_L t} \quad (2)$$

where, after disregarding anti-resonant terms (rotating wave approximation), $\tilde{\mathbf{P}}(\mathbf{r}, t) = \sum_i \delta(\mathbf{r} - \mathbf{r}_i) \mathbf{d} \tilde{\rho}_{01}^i(t)$. We show in the Supplemental Materials that the radiative Rabi frequency $\chi_{Rad} = \mathbf{d} \cdot \tilde{\mathfrak{F}}\{\tilde{\mathbf{P}}\}/\hbar$ can be written as $\chi_{Rad} = -(\Omega + i\gamma)$, where γ is a decay term and Ω is an energy shift. Both terms are proportional to $\Gamma = d^2 \omega_L^3 / 3\epsilon \hbar \pi c^3$, which corresponds to the spontaneous decay rate of each dot for $\omega_L = \omega_0$. This parameter provides a lower bound on decay rates, which can include contributions from other processes (e.g. phonons or Auger processes). In particular, the conditions $1/T_1 > \Gamma$ and $1/T_2 > \Gamma/2$ must hold.

The numerical model thus consists of a system of coupled, time-delayed nonlinear Liouville's equations where the right-hand side depends on the derivatives of $\tilde{\mathbf{P}}(t)$ up to the second order. Standard methods for solving this system of equations—such as RK4—are unstable. Our approach comprises adapting methods from discretizing time domain integral equations [19] and coupling these with a predictor corrector scheme to obtain a solution to the coupled Liouville equations [13, 18]. At a given timestep t_n , the algorithm guesses a value for $\tilde{\rho}^i(t_{n+1})$, then evaluates $\tilde{\mathfrak{F}}\{\tilde{\mathbf{P}}(t_{n+1})\}$ and $\tilde{\rho}^i(t_{n+1})$ to update $\tilde{\rho}^i(t_{n+1})$ until convergence. Repeating this process for each timestep marches the function forward to obtain a solution for all times.

Results. In this section, we illustrate the capabilities of our computational approach by simulating ensembles of quantum dots embedded in solid media. In all simulations, an incident field with the shifted Gaussian waveform:

$$\mathbf{E}_L(\mathbf{r}, t) = E_0 e^{-\frac{(\mathbf{k} \cdot \mathbf{r} - \omega_L(t-t_0))^2}{2\sigma^2}} \cos \omega_L t \hat{\mathbf{x}}. \quad (3)$$

is used to excite an ensemble of dots lying initially in the ground state $(\tilde{\rho}_{00}, \tilde{\rho}_{01})|_{t=0} = (1, 0)$. Here $\omega_L \approx 4823.67 \text{ ps}^{-1}$, $\sigma/\omega_L \approx 0.3446 \text{ ps}$, $\mathbf{k} = \omega_L/c \hat{\mathbf{z}}$, and the laser amplitude E_0 is adjusted to produce a π -pulse on

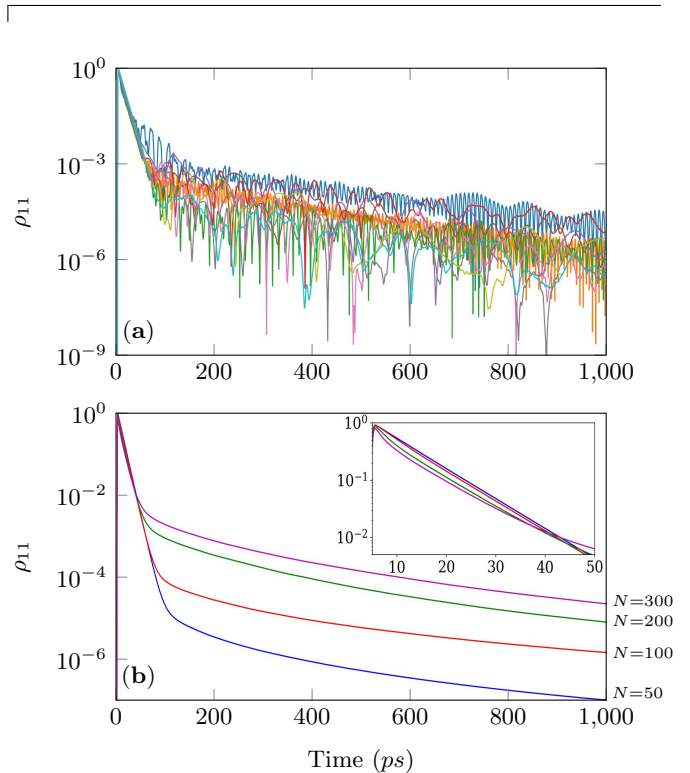


FIG. 1. Time evolution of the population excitation ρ_{11} for a Gaussian distribution of dots with $d/d_0 = 1.0$. (a) Per-dot time evolution for $N = 200$ (10 dots shown). (b) Dot-averaged values for different N . (b, Inset) Immediately post-excitation, a faster decay is observed for larger N .

a single dot. First, we consider the case of identical dots with $\omega_0^i = \omega_L$. The resonant pulse is chosen to peak at $t_0 = 5 \text{ ps}$. The systems of N quantum dots are assumed to be embedded in a NaCl medium with refractive index $n \approx 1.54$. They are Gaussian-distributed with a standard deviation along each dimension of 0.5λ . This fixed spread implies that the dot density increases with N . Each dot has an identical dipole moment $\mathbf{d} = d\hat{\mathbf{x}}$, which is varied based on a reference dipole moment of strength $d_0/e \approx 0.002536 \mu\text{m}$. For each value of d , the decay times T_1 and $T_2 = 2T_1$ are modified to satisfy $1/T_1 > \Gamma$.

Fig. 1a depicts the time behavior of a set of ten dots chosen from a simulation with $N = 200$ dots, portraying a rich phenomenology of oscillations following the initial excitation. These oscillations result from local energy shifts induced by randomly distributed neighboring dots and are dominated by the $1/R^3$ contribution from Eq. (1). Immediately post-excitation, we observe a weak superradiant behavior, which can be seen in Fig. 1b

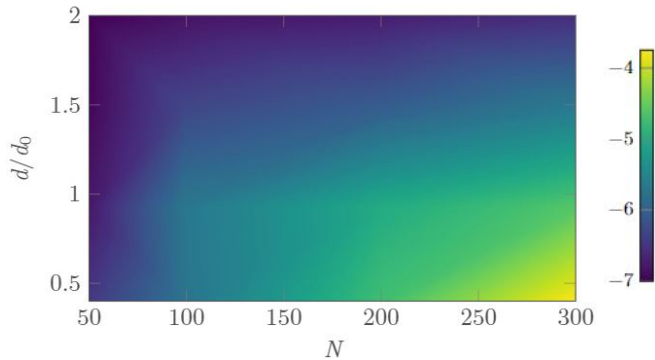


FIG. 2. Log-plot of averaged-over-trials population ρ_{11} at 1 ns as a function of dipole strength and N .

where we show the population dynamics averaged over all dots for different N . The figure and inset show a faster re-emission after pulse excitation in configurations with a greater density of emitters. Nonetheless, the ideal N^2 dependence of the enhancement is strongly reduced due to random dot interactions. Afterward, the system settles into a subradiant regime where re-emission slows down. This transition is visible in both per-dot (Fig. 1a) and averaged (Fig. 1b) plots. Higher emitter density also leads to more subradiance, resulting in more significant population trapping at long times. Increasing the dipole strength d , while increasing the strength of interactions, also forces shorter decay times. Hence, the net effect is a reduction in population trapping, which is displayed in Supplemental Fig. 1. Fig. 2 summarizes the effects of N and d on the average population at 1 ns. The subradiant population trapping is enhanced by larger N and lower d , corresponding to dense systems of weakly interacting dots.

Further patterns emerge when examining the radiated field of Eq. (1). Field intensities in the region external to the dot cloud show patterns with a period of half the wavelength (Fig. 3). As the excitation pulse propagates along z , we also observe a clear enhancement of the emission along the positive z axis, a well-known signature of collective radiative emission [20]. The intensity along the y -axis, shown in Supplemental Fig. 2, indicates that the patterns persist for stronger dipole values. It is worth noting that the three terms of Eq. (1) are not all commensurate. While the near-field interaction terms produce a random pattern near the origin, the far-field $1/R$ term produces a regular pattern characterized by phase shifts in some directions.

Time-space plots reveal the synchronization of groups of dots into temporal oscillations in Fig. 4, where we plot the intensity along the y -axis as a function of time. These oscillations become more pronounced and irregular with increased dipole strength and dot density. This effect is captured in Supplemental Fig. 3, which displays the tem-

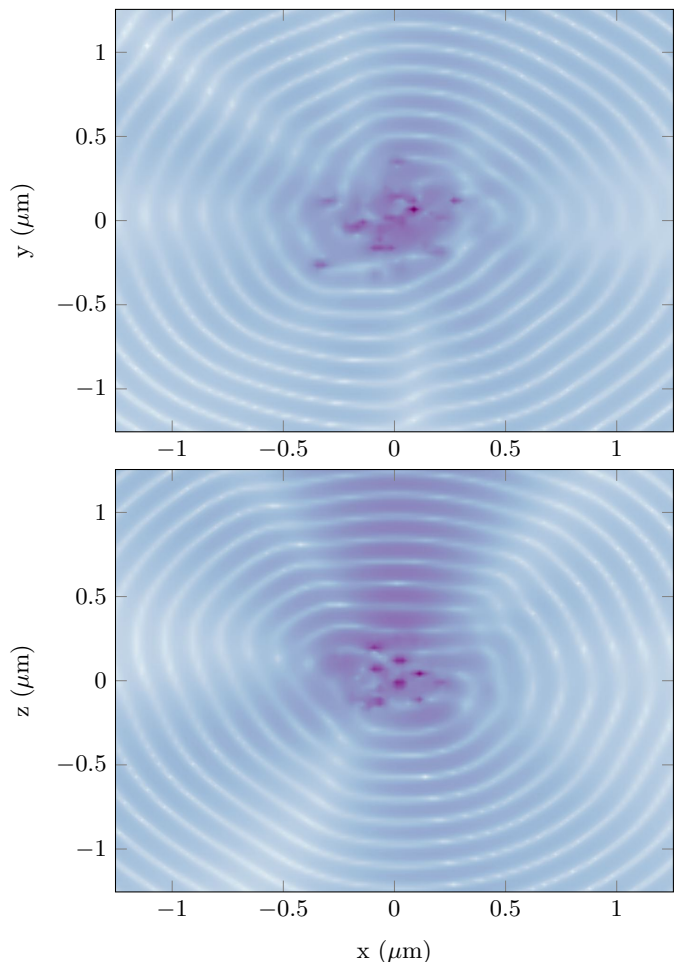


FIG. 3. Colormaps of logarithmic field intensities for a configuration with $N = 100$ and $d/d_0 = 1.00$ after 20 ps, on the $x-y$ (top) and $x-z$ (bottom) planes. The spatial oscillations occur with a period about half the wavelength of 253 nm. Also note the enhancement along the laser propagation direction in the positive z axis.

poral Fourier transforms of the field intensity along the y -axis for different dipole strengths. The Fourier transform shows that additional peaks emerge in the emission corresponding to new oscillation periods in the dot ensemble when the dipole increases.

Additionally, we studied the effect of inhomogeneous broadening by considering dots with energy $\hbar\omega_0^i$ that follow a Gaussian distribution of width δ centered at ω_L . Increasing δ affects the dynamics in two ways: (1) the excitation induced by the π pulse is less efficient, so the population inversion decreases, and (2) the population of subradiant modes increases due to increased disorder. These two competing effects can be seen in Fig. (5). The average excitation of the dots right after excitation decreases with δ , but at longer times, its dependence on the inhomogeneity is characterized by a peak around $\hbar\delta = 0.1$ meV. The full dependence of the subradiant

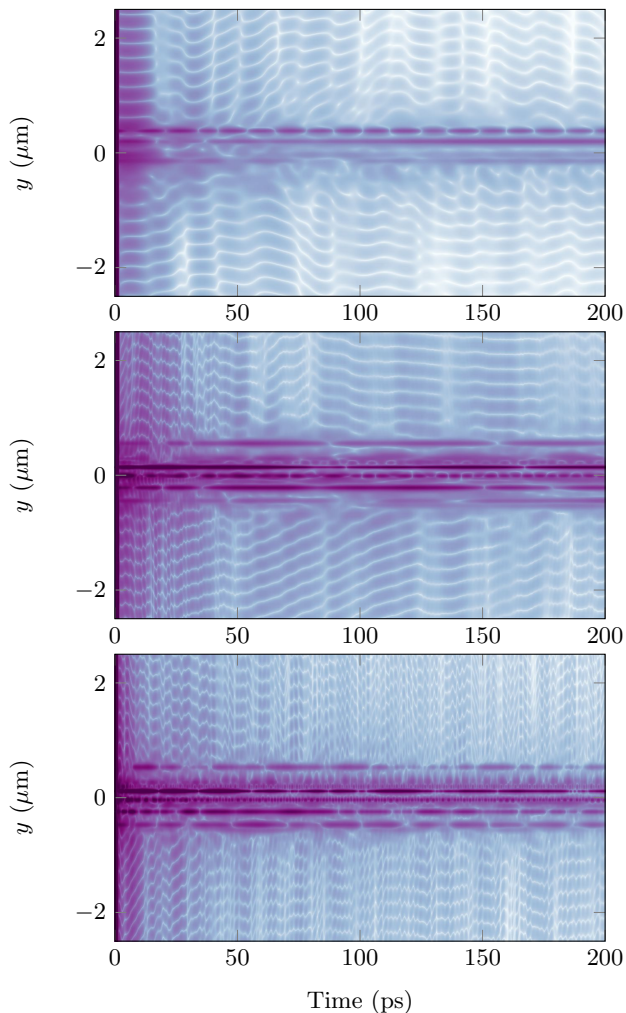


FIG. 4. Plot of logarithmic radiated field intensities for $N = 100$, $d/d_0 = 1.0$ (top), $N = 200$, $d/d_0 = 1.0$ (middle), $d/d_0 = 2.0$ (bottom) in time and space. Evident are not only spatial but temporal oscillations, becoming enhanced for larger values of the dipole moment. It is also evident that the intensity amplitude increases with the number of emitters. Groups of dots in the cloud ($y \sim 0$) undergo emission synchronization leading to periodic oscillations that become more irregular as the density increases.

trapping on δ and N is shown in Supplemental Fig. 4.

Discussion. Our computational approach and software available in [9] allows us to understand the transient response of ensembles of optical emitters following a laser pulse excitation. We observe superradiant and subradiant emission, and synchronized oscillations. Long-established studies have shown the usefulness of semiclassical models of superradiance [20, 21]. However, by accounting for the mutual coupling of emitters, our formulation precisely describes local field inhomogeneity, which reduces the superradiant emission in favor of configuration-dependent subradiant emission. We found that, due to electromagnetic coupling and spatial ran-

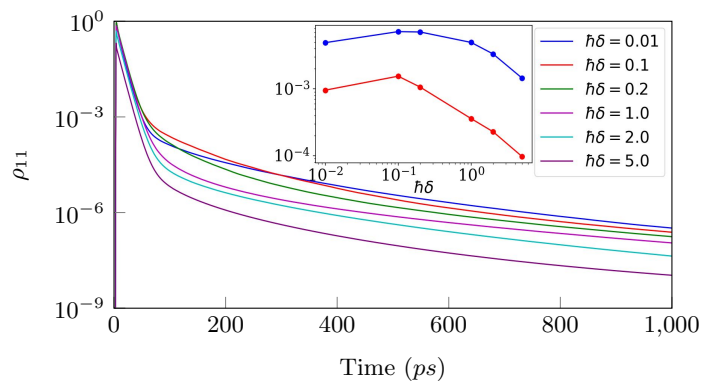


FIG. 5. Time evolution of space-averaged population excitation ρ_{11} for the same $N = 200$ distribution as Figure 1, for different inhomogeneous broadening values δ (in meV). (Inset) Excitation values as a function of δ , at $t = 500$ ps (blue) and $t = 1000$ ps (red). It is evident that broadening tends to reduce population trapping at long times.

domness, superradiance is fragile even in the presence of identical emitters for ensembles of size comparable to $\lambda/2$. Subradiance, on the other hand, leads to a build-up of slowly decaying population inversion, which is maximized at small dipole values and large density, as shown in Fig. 5. Our findings are consistent with recent experiments in Rydberg atoms where the atom-atom electromagnetic coupling led to superradiance decoherence [22], and the significant deviations observed in quantum dots [17] from the ideal N^2 dependence. When decaying, groups of dots exhibit synchronized oscillations that become more irregular and for larger dipoles and density, suggesting transitions towards chaotic dynamics [23]. Energy inhomogeneous broadening contributes to the suppression of superradiance in favor of subradiance. However, we found that the subradiance emission peaks at small levels of energy broadening, as the overall population inversion created by a pulse decreases for large broadening (Fig. 5). These findings could help design optical systems where highly-entangled subradiant collective states dominate the light emission.

Acknowledgements. This work was supported by the National Science Foundation grant OAC1835267 and by Michigan State University through computational resources provided by the Institute for Cyber-Enabled Research. We thank Drs. C. Glosser and M. Maghrebi for enlightening discussions.

-
- [1] M. O. Scully and A. A. Svidzinsky, The Super of Superradiance, *Science* **325**, 1510 (2009).
 - [2] K. Cong, Q. Zhang, Y. Wang, G. T. Noe, A. Belyanin, and J. Kono, Dicke superradiance in solids, *JOSA B* **33**, C80 (2016).

- [3] O. Hess and T. Kuhn, Maxwell-Bloch equations for spatially inhomogeneous semiconductor lasers. I. Theoretical formulation, *Physical Review A* **54**, 3347 (1996).
- [4] C. Jirauschek, M. Riesch, and P. Tzenov, Optoelectronic device simulations based on macroscopic Maxwell-Bloch equations, *Advanced Theory and Simulations* **2**, 1900018 (2019).
- [5] M. Gross and S. Haroche, Superradiance: An essay on the theory of collective spontaneous emission, *Physics reports* **93**, 301 (1982).
- [6] R. Friedberg, S. Hartmann, and J. Manassah, Limited superradiant damping of small samples, *Physics Letters A* **40**, 365 (1972).
- [7] A. Asenjo-Garcia, M. Moreno-Cardoner, A. Albrecht, H. Kimble, and D. E. Chang, Exponential improvement in photon storage fidelities using subradiance and “selective radiance” in atomic arrays, *Physical Review X* **7**, 031024 (2017).
- [8] A. Piñeiro Orioli, J. K. Thompson, and A. M. Rey, Emergent dark states from superradiant dynamics in multi-level atoms in a cavity, *Phys. Rev. X* **12**, 011054 (2022).
- [9] E. Lu, C. Glosser, C. Piermarocchi, and B. Shanker, [QuEST:doi.org/10.5281/zenodo.6499556](https://doi.org/10.5281/zenodo.6499556) (2022).
- [10] C. Glosser, B. Shanker, and C. Piermarocchi, Collective rabi dynamics of electromagnetically coupled quantum-dot ensembles, *Physical Review A* **96**, 033816 (2017).
- [11] J. Hoskins, J. Kaye, M. Rachh, and J. C. Schotland, A fast, high-order numerical method for the simulation of single-excitation states in quantum optics (2021), [arXiv:2109.06956 \[math.NA\]](https://arxiv.org/abs/2109.06956).
- [12] J. Kraisler and J. C. Schotland, Collective spontaneous emission and kinetic equations for one-photon light in random media, *Journal of Mathematical Physics* **63**, 031901 (2022).
- [13] C. Glosser, E. Lu, T. Bertus, C. Piermarocchi, and B. Shanker, Acceleration techniques for semiclassical Maxwell-Bloch systems: An application to discrete quantum dot ensembles, *Computer Physics Communications* **258**, 107500 (2021).
- [14] G. Rainò, M. A. Becker, M. I. Bodnarchuk, R. F. Mahrt, M. V. Kovalenko, and T. Stöferle, Superfluorescence from lead halide perovskite quantum dot superlattices, *Nature* **563**, 671 (2018).
- [15] K. Miyajima, Y. Kagotani, S. Saito, M. Ashida, and T. Itoh, Superfluorescent pulsed emission from biexcitons in an ensemble of semiconductor quantum dots, *Journal of Physics: Condensed Matter* **21**, 195802 (2009).
- [16] K. Miyajima, K. Maeno, S. Saito, M. Ashida, and T. Itoh, Biexcitonic superfluorescence from CuCl quantum dots under resonant two-photon excitation, *physica status solidi c* **8**, 209 (2011).
- [17] M. Scheibner, T. Schmidt, L. Worschech, A. Forchel, G. Bacher, T. Passow, and D. Hommel, Superradiance of quantum dots, *Nature Physics* **3**, 106 (2007).
- [18] A. Glaser and V. Rokhlin, A new class of highly accurate solvers for ordinary differential equations, *Journal of Scientific Computing* **38**, 368 (2009).
- [19] B. Shanker, M. Lu, J. Yuan, and E. Michielssen, Time domain integral equation analysis of scattering from composite bodies via exact evaluation of radiation fields, *IEEE Transactions on Antennas and Propagation* **57**, 1506 (2009).
- [20] N. E. Rehler and J. H. Eberly, Superradiance, *Physical Review A* **3**, 1735 (1971).
- [21] C. Stroud Jr, J. Eberly, W. Lama, and L. Mandel, Superradiant effects in systems of two-level atoms, *Physical Review A* **5**, 1094 (1972).
- [22] E. Suarez, P. Wolf, P. Weiss, and S. Slama, Superradiance decoherence caused by long-range rydberg-atom pair interactions, *Physical Review A* **105**, L041302 (2022).
- [23] C. Liu, A. Di Falco, and A. Fratalocchi, Dicke phase transition with multiple superradiant states in quantum chaotic resonators, *Phys. Rev. X* **4**, 021048 (2014).